ChemComm

COMMUNICATION

View Article Online
View Journal | View Issue

Open Access Article. Published on 15 November 2022. Downloaded on 1/15/2026 11:20:44 PM.
This article is licensed under a Creative Commons Attribution 3.0 Unported Licence.

Check for updates

Cite this: *Chem. Commun.*, 2022, **58**, 13628

Received 13th August 2022,
Accepted 15th November 2022

DOI: 10.1039/d2cc04510a

rsc.li/chemcomm

Selective gas adsorption by calixarene-based porous octahedral M_{32} coordination cages†

Ivan V. Khariushin,[ab] Alexander S. Ovsyannikov,*[c] Stéphane A. Baudron,[a] Jas S. Ward,[d] Anniina Kiesilä,[d] Kari Rissanen,[d] Elina Kalenius,[d] Konstantin A. Kovalenko,[e] Vladimir P. Fedin,[e] Svetlana E. Solovieva,[b] Igor S. Antipin,[b] Véronique Bulach[a] and Sylvie Ferlay*[a]

Giant octahedral M_{32} coordination cages were prepared *via* self-assembly of sulfonylcalix[4]arene-supported tetranuclear M(II) clusters (M = Co, Ni) with hybrid linker based on tris(dipyrrinato)cobalt(III) complexes appended with peripherical carboxylic groups. Due to intrinsic and extrinsic porosity, the obtained solid-state supramolecular architectures demonstrated good performance as adsorbents for the separation of industrially important gases mixtures.

Molecular coordination cages or polyhedra[1–3] are drawing attention, due to their intriguing architectures and unique physical and chemical properties which can be tuned by a judicious choice of their constituents: metal ions or clusters and connectors. Such molecular structures presenting intrinsic porosity in the crystalline phase may find applications in the field of molecular separation/storage,[4,5] sensing,[6,7] catalysis,[8,9] and drug delivery.[10] Contrary to metal–organic frameworks (MOFs), these discrete coordination compounds can be soluble, offering potential advantages in synthesis, homogeneous catalysis, purification and processing.[11–13] The void space within the coordination cages determines uptake/release of guest molecules through weak and reversible interactions, which is crucial for catalysis for example, and the flexible space between the cavities allows also the adsorption of a large quantity of small molecules. However, understanding and optimizing porosity in such solids is challenging, since it results from many parameters. The use of intrinsic porous components, like macrocyclic preformed molecules, can be a key point for the formation of highly porous molecular cages, for selective gas adsorption.

Calix[4]arenes[14,15] are a very attractive macrocyclic building block because of the presence of the hydrophobic cavity composed of four aromatic rings adopting different conformations, which, therefore, can be used to accommodate different organic molecules or gases.[16,17] Among the different available derivatives, tetrasulfonylcalix[4]arene (**1-4H**),[18] represents an ideal polydentate ligand to form coordination clusters,[19,20] capsules or (super)containers,[21,22] and cages.[23–25] The three-component approach involving **1-4H** (Fig. 1), metallic cations, and polytopic carboxylate ligands **L** has been successfully used for the reproducible formation of polyhedral cages, involving the $[\mathbf{1}\text{–}M^{II}_4(\mu_4\text{-}H_2O)]^{4+}$ building blocks (M = Co, Ni or Zn, described as a "shuttlecock" component).[20] Based on the use of **1-4H**, and different connectors (generally linear or presenting a D_{3h} geometry), molecular coordination cages presenting various nuclearities and shapes have been reported: dimeric M_8,[26] square-like M_{16},[27,28] and octahedral M_{24}[28–35] nanosized cages possessing appealing catalytic properties and also drug delivery abilities. Some gas adsorption properties together with selectivity have been reported for octahedral M_{24}[36,37] or larger calixarene based cages, related to the flexible internal and external porosity.[38,39] Till now, only one example of calixarene based octahedral cages

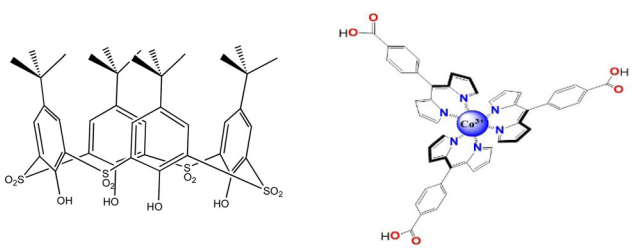

Fig. 1 Tetrasulfonylcalix[4]arene (**1-4H**) and *rac*-tris(dipyrrinatocarboxylic)-cobalt(III) complex (**$Co^{III}L_3$-3H**) as building blocks for the formation of cages.

[a] Université de Strasbourg, CNRS, CMC UMR 7140, F-67000 Strasbourg, France. E-mail: ferlay@unistra.fr
[b] Kazan Federal University, Kremlevskaya 18, Kazan 420008, Russian Federation
[c] Arbuzov Institute of Organic and Physical Chemistry, FRC Kazan Scientific Center, Russian Academy of Sciences, Arbuzova 8, Kazan, Russian Federation
[d] University of Jyvaskyla, Department of Chemistry, Survontie 9 B, 40014, Jyväskylä, Finland
[e] Nikolaev Institute of Inorganic Chemistry, Siberian Branch of the Russian Academy of Sciences, 3, Acad. Lavrentiev Ave., Novosibirsk, 630090, Russian Federation

† Electronic supplementary information (ESI) available: Synthesis of cages, Single X-ray diffraction details, IR, IM-MS, PXRD, TGA measurements and details concerning gas adsorption and gas selectivity measurements. CCDC 2192093 and 2192095. For ESI and crystallographic data in CIF or other electronic format see DOI: https://doi.org/10.1039/d2cc04510a

This journal is © The Royal Society of Chemistry 2022

Open Access Article. Published on 15 November 2022. Downloaded on 1/15/2026 11:20:44 PM.
This article is licensed under a Creative Commons Attribution 3.0 Unported Licence.

incorporating a metallic connector has been reported,[34] and for this type of M_{32} cages, the porous properties have not been reported.

We report herein on the synthesis and complete structure elucidation of the formation of racemic octahedral cages, based on the use of tetrasulfonylcalix[4]arene and metallic dipyrrin connectors (Fig. 1). Two isostructural examples of such species are presented and fully structurally characterized, together with their unique gas adsorption and selectivity behaviour. Dipyrrin complexes have demonstrated their high stability and propensity to form discrete coordination species including cage-like architectures or polymeric coordination assemblies (MOFs) in the crystalline phase displaying especially attractive tuneable photoelectric conversion abilities.[40–42]

The monometallic dipyrrin based connectors tris(dipyrrinato-carboxylic)cobalt(III) $(Co^{III}\mathbf{L}_3)^{3-}$ (**L** = 5-(4-carboxyl-phenyl)-4,6-dipyrrinato)) were obtained in a racemic form following the reported procedure.[43,44] Subsequently, the one-pot three-component approach for obtaining octahedral cages was performed with a 4 : 3 : 12 mixture of $(Co^{III}\mathbf{L}_3)^{3-}$, **1-4**H, and $M^{II}(Cl)_2{\cdot}6H_2O$ (M = Co or Ni) with Et_3N (30 eq.) in a 1/1 *N*,*N*-dimethylformamide (DMF) and MeOH mixture. Using the slow diffusion technique (see experimental part in ESI†) at ambient temperature led to single crystals in 86% yield. The crystalline compounds were isolated and characterized by a variety of techniques including single-crystal X-ray diffraction (XRD), thermogravimetric analysis (TGA), IR spectroscopy, ion mobility mass spectrometry (IM-MS). The crystals are soluble in dichloromethane.

A single-crystal XRD study unambiguously revealed the formation of neutral isostructural octahedral cages of formula $[\mathbf{1}{-}M^{II}_4(\mu_4{-}H_2O)]_6[Co^{III}\mathbf{L}_3]_8{\cdot}(DMF)_n{\cdot}(H_2O)_n$ (**2**, M = Co $(Co^{II}_{24}Co^{III}_8)$ and **3**, M = Ni $(Ni^{II}_{24}Co^{III}_8)$) (Fig. 2). Compounds **2** and **3** are isomorphous and crystallize in the centrosymmetric $R\bar{3}c$ trigonal space group and the asymmetric unit is shown in Fig. S1 (ESI† together with the crystallographic Table S1). The $(Co^{III}\mathbf{L}_3)^{3-}$ carboxylate connectors are present as a recemic mixture, displaying an equal amount of lambda and delta complexes in the crystal. The cages are formed of 6 $[\mathbf{1}{-}M^{II}_4(\mu_4{-}H_2O)]^{4+}$ moieties, forming the vertices of the octahedron, and 8 $(Co^{III}\mathbf{L}_3)^{3-}$ units, located on the 8 faces of the octahedron, and thus connecting 3 vertices each (Fig. 2), as already observed using D_{3h} tricarboxylic connectors.[29,30] In the $[\mathbf{1}{-}M^{II}_4(\mu_4{-}H_2O)]^{4+}$ shuttlecock-like moieties, each M^{II} cation (M = Co or Ni) is in an octahedral O6 environment, coordinated to one sulfonyl and two oxygen atoms from the fully deprotonated $\mathbf{1}^{4-}$ units, two oxygen atoms from $(Co^{III}\mathbf{L}_3)^{3-}$ carboxylate connectors and one oxygen atom from μ_4-H_2O atom (as shown in Fig. S2, ESI†). Due to the presence of both Δ and Λ enantiomers, disorder is observed in the N6 environment around the Cobalt(III) cations of the $(Co^{III}\mathbf{L}_3)^{3-}$ carboxylate connectors. Some of the *tert*-butyl groups of $\mathbf{1}^{4-}$ are also disordered. During the refinement, a BYPASS solvent mask within Olex2 was applied,[45] therefore the solvents lying in and between the cages were not modelled.

The dimensions of the symmetrical cage are approximately 46 × 46 × 46 Å^3 for **2** and **3** and the inner cavity has a diameter of *ca.* 19 Å. Calculations using PLATON[46] show that **2** and **3** have approximately 68% of the total volume available for guest inclusion or gas adsorption.

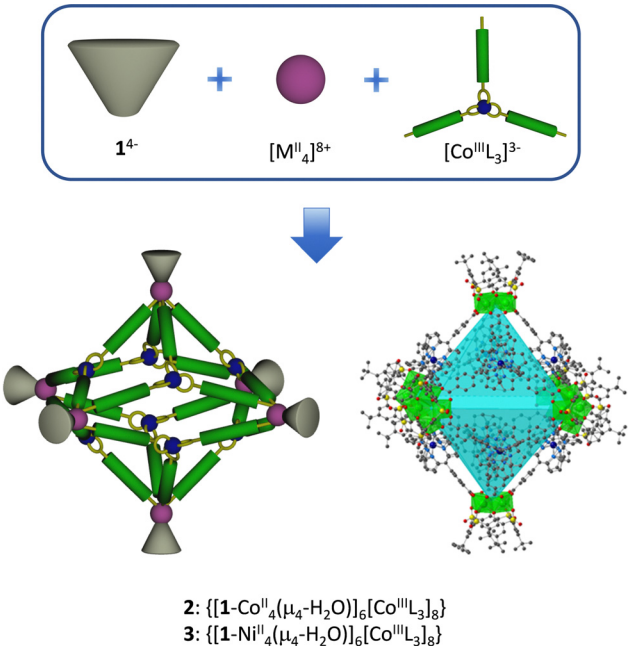

Fig. 2 The three-component approach leading to the formation of octahedral cages **2** and **3**. On the bottom, the representation of a cage from X-ray diffraction data. M^{II} cations in the $[\mathbf{1}{-}M^{II}_4(m_4{-}H_2O)]^{4+}$ species are represented as green polyhedra and the faces of the octahedron are colored in blue. The $(Co^{III}\mathbf{L}_3)^{3-}$ connectors are located above the faces of the octahedron.

In the unit-cell, the cages are packed in an hexagonal fashion in the *x*O*y* plane and aligned parallelly along the *b* axis. Along the *c* axis, they display a rotation, so that they are not superimposable, as shown in Fig. 3.

ESI-MS experiments on negative polarization, show abundant single peak distributions for both samples **2** and **3** on *m*/*z* range ∼2210–2230, which correspond to intact cages on charge state 6^- with some H_2O_n/DMF_n adduct formation (Fig. S4, ESI†). The base peaks in distribution result in molecular weights of 13 365 Da and 13 346 Da for **2** and **3**, respectively, which compares well with theoretical MWs of empty cages (13 249 Da for **2** and 13 243 Da for **3**). IM-MS arrival time

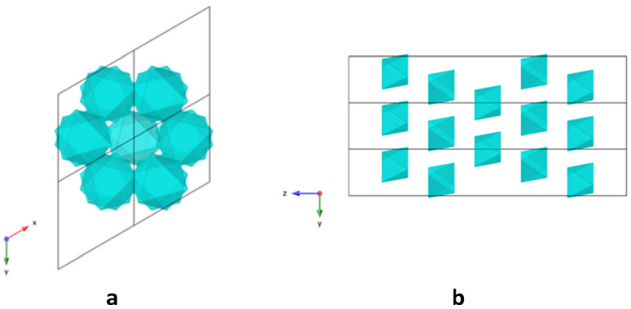

Fig. 3 The schematic view for the packing of **2** (and **3**) in the unit cell (a) in the *x*O*y* plane (b) in the *y*O*z* plane. Blue color represents the faces of the octahedron formed by the M_{32}-cages.

Open Access Article. Published on 15 November 2022. Downloaded on 1/15/2026 11:20:44 PM.
This article is licensed under a Creative Commons Attribution 3.0 Unported Licence.

distributions show single drift peaks with similar drift times for both cages, which result in collision cross section ($^{DT}CCS_{N2}$) values of 1879 Å^2 and 1855 Å^2 for cages **2** and **3**, respectively. These values have an excellent correlation to theoretical, single-crystal XRD structure-driven $^{EHSS}CCS_{N2}$ value (1834.3 Å^2 for empty cages **2** and **3**). This not only evidences the structural similarity between the two cages, but also consolidates structural similarity to solid state structure.

The TGA traces (see Fig. S5 and S6 in ESI†) confirm the presence of solvents in the unit cell, and a loss of 21.7% in mass and 25.4% for **2** and **3** respectively that corresponds to the departure of MeOH, DMF and adsorbed H_2O located within and outside the cage. The resulting activated cages display much lower loss of mass, only due to the re-adsorption of the water molecules from air. This accounts for the fact that **2** and **3** are hygroscopic. The data clearly shows that **2** and **3** are thermally stable up to 360 °C when desolvated.

The PXRD patterns of **2** and **3** (see Fig. S7, ESI†) attest for the decomposition of the crystal arrangement of discrete cage species after separation from the mother liquor, induced by the release of solvent molecules, which can be seen as the beginning of the amorphization process. This fact has been frequently observed for large coordination porous species,[34,36] but generally without damage for the coordination cages. The stability of the obtained cages was confirmed by FT-IR-studies of freshly prepared, activated samples (see Fig. S3a and b, ESI†).

As already mentioned, the accessible space inside the M_{32} cages and in the unit cell (intrinsic and extrinsic porosity) of **2** and **3** may accommodate guest molecules and this was investigated. The permanent porosity of the activated compounds **2** and **3** (dynamic vacuum at 180 °C for 6 h, see Experimental section in ESI†) was examined by N_2 uptake measurement at 77 K, revealing a type-I isotherm presenting a small hysteresis (see Fig. S8, ESI†) indicating a microporous material with Brunauer–Emmett–Teller and Langmuir surface areas of 417 (445) and 462 (506) m^2 g^{-1}, for **2** (**3**), respectively (see Table S2, ESI†). The presence of the hysteresis is probably due to the extrinsic porosity of the compounds. The pore size distributions were calculated using a QSDFT approach (see Fig. S9, ESI†) and show the presence of one type of narrow pores for **2** and two types of narrow pores in **3**, which is in a good agreement with their observed crystalline structures and their flexible extrinsic microporosity. Compound **2** contains irregular mesopores probably due to mesostructuring of crystallites because of their small sizes.

Isotherms of low-pressure adsorption (at pressure region up to 1 bar) of other small molecules like CO_2, CH_4, C_2H_2, C_2H_4 and C_2H_6 at 273 and 298 K were measured (see Fig. 4). For all gases, the saturation in the experimental pressure range is not observed. The gas uptakes obtained for **2** and **3** at 273 and 298 K are presented in Table S3 (ESI†). Best results obtained for **2** and **3** reveal a maximum CO_2 uptake of 7.4 and 7.7 wt%, respectively, at 273 K and a pressure of 1 bar (see Table S4, ESI†). The isosteric heats (Qst) of adsorption for each gas have been calculated by means of virial approach (see Table S5, ESI†) and values of zero-coverage heats of adsorption are of 7.0 (7.2) kJ mol^{-1} for N_2, 11.7 (14.8) kJ mol^{-1} for CH_4,

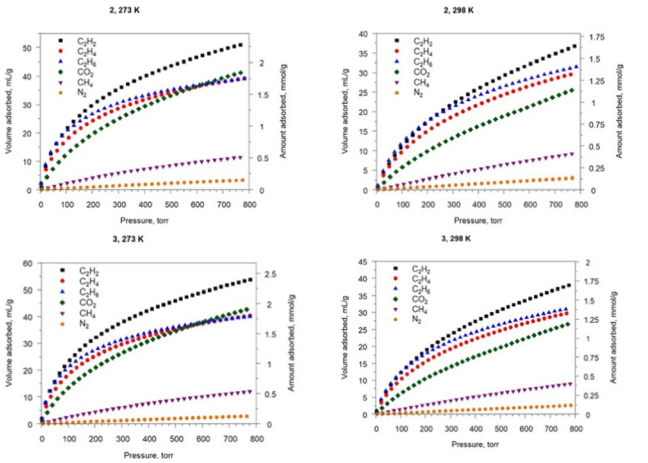

Fig. 4 Gas sorption isotherms for **2** (top) and **3** (bottom) at 273 K (left) and 298 K (right) between 0 and 800 torr (1.07 bar). Desorption isotherms branches are omitted for clarity due to negligible adsorption–desorption hysteresis (Fig. S10, ESI†).

28.0 (29.1) kJ mol^{-1} for CO_2, 28.7 (31.0) kJ mol^{-1} for C_2H_6, 27.4 (29.4) kJ mol^{-1} for C_2H_4 and 29.4 (31.4) kJ mol^{-1} for C_2H_2 on **2** (**3**), respectively. Compounds **2** and **3** exhibit much higher adsorption capacities for CO_2, C_2H_2, C_2H_4 and C_2H_6 compared to those observed for CH_4. This fact is in a good agreement with the calculated heats of adsorption (see Table S7, ESI†), which suggest that these compounds possessing selective adsorption of different gas mixtures can even be used for the separation of industrially important gas mixtures.

The Ideal Adsorbed Solution Theory (IAST)[47] selectivities for 50 : 50 and 5 : 95 C_2H_6/CH_4 binary mixture adsorption are 18.7 (18.6) and 75.4 (75.0) for **2** (**3**) at 273 K, and for 50 : 50 and 5 : 95 C_2H_2/CH_4 binary mixture adsorption are 18.3 (19.6) and 75.6 (82.6) for **2** (**3**) (see Table S8 and Fig. S14–S20, ESI†). To the best of our knowledge, the selective adsorption of light hydrocarbon on porous coordination cages is still poorly described in the literature, and compounds **2** and **3** demonstrate remarkable IAST selectivities even among representative MOFs (see Tables S9 and S10, ESI†). Moderate-to-high selectivity was also demonstrated for compounds **2** and **3** for other evaluated mixtures. Good adsorption selectivity is observed for a C_2H_2/CO_2 mixture which is highly difficult to separate due to close physical characteristics of these gases. Additionally, high adsorption selectivity is observed for CO_2/CH_4 and CO_2/N_2 mixtures, which are important for natural gas upgrading and flue gas separation. The preferred adsorption of C_2H_6 over C_2H_4 should also be noted, which is unusual, as there is still a moderate number of examples of such compounds among MOFs and none among coordination cages. However, the selectivity factors towards C_2H_6/C_2H_4 mixture for both **2** and **3** are quite low. **2** and **3** are therefore good candidates for further studying the separating properties, especially towards C_2H_2/CH_4 and C_2H_6/CH_4 mixtures.

In summary, we have described a convenient and reliable approach for the design and synthesis of racemic porous octahedral giant coordination cages resulting from the three-component

Open Access Article. Published on 15 November 2022. Downloaded on 1/15/2026 11:20:44 PM.
This article is licensed under a Creative Commons Attribution 3.0 Unported Licence.

assembly of sulfonated calixarene, tris-dipyrrin complex and metallic cations. In addition, it was revealed that the obtained supramolecular architectures, which incorporate 32 metal cations and possess large cavities (*ca.* 19 Å), when activated, exhibit highly selective adsorption of C_2-hydrocarbon gases *versus* CH_4. This is the first report providing a new approach for rational design of such supramolecular materials with respect to targeted functionalization (adsorption, chiral separation, light-harvesting, luminescence, magnetism *etc.*). The synthesis of new coordination cages using self-assembly of tetranuclear calix[4]arene clusters with other metal–organic linkers is currently under investigation.

This work was supported by the University of Strasbourg, the Institute Universitaire de France, Doctoral Mechnikov scholarship from French Embassy (I. V. K.), the CNRS, the Russian Science Foundation (Project N° 19-73-20035 to I. V. K., A. S. O., S. E. S., I. S. A.), the Government assignment for Nikolaev Institute of RAS (K. A. K., V. P. F.). The authors are grateful to Kurchatov Complex For Synchrotron And Neutron Investigations for performing of XRD-analysis on powdered samples (Dr Roman D. Svetogorov), to Spectral-Analytical Center of FRC Kazan Scientific Center of RAS for their help and support in TGA (Dr Ayrat R. Khamatgalimov) and IR studies. The authors gratefully acknowledge the Magnus Ehrnrooth Foundation (J. S. W.), the Academy of Finland (K. R. grant N° 317259), and the University of Jyväskylä, Finland, for financial support.

Conflicts of interest

There are no conflicts to declare.

Notes and references

1 D. J. Tranchemontagne, Z. Ni, M. O'Keeffe and O. M. Yaghi, *Angew. Chem., Int. Ed.*, 2008, **47**, 5136–5147.
2 T. R. Cook and P. J. Stang, *Chem. Rev.*, 2015, **115**, 7001–7045.
3 E.-S. M. El-Sayed and D. Yuan, *Chem. Lett.*, 2020, **49**, 2853.
4 E. J. Gosselin, C. A. Rowland and E. D. Bloch, *Chem. Rev.*, 2020, **120**, 8987–9014.
5 I. S. Antipin, *et al.*, *Russ. Chem. Rev.*, 2021, **90**, 895.
6 X. Zhang, W. Wang, Z. Hu, G. Wang and K. Uvdal, *Coord. Chem. Rev.*, 2015, **284**, 206–235.
7 H.-Y. Li, S.-N. Zhao, S.-Q. Zang and J. Li, *Chem. Soc. Rev.*, 2020, **49**, 6364–6401.
8 D. M. Kaphan, M. D. Levin, R. G. Bergman, K. N. Raymond and F. D. Toste, *Science*, 2015, **350**, 1235–1238.
9 W. Cullen, M. C. Misuraca, C. A. Hunter, N. H. Williams and M. D. Ward, *Nat. Chem.*, 2016, **8**, 231–236.
10 J.-S. M. Lee, K.-I. Otake and S. Kitagawa, *Coord. Chem. Rev.*, 2020, **421**, 213447.
11 E. G. Percástegui, T. K. Ronson and J. R. Nitschke, *Chem. Rev.*, 2020, **120**(24), 13480–13544.
12 E. G. Percástegui, *Chem. Commun.*, 2022, **58**, 5055.
13 S. Lee, H. Jeong, D. Nam, M. S. Lah and W. Choe, *Chem. Soc. Rev.*, 2021, **50**, 528–555.
14 C. D. Gutsche, *Calixarenes Revised: Monographs in Supramolecular Chemistry*, The Royal Society of Chemistry, Cambridge, 1998, vol. 6.
15 A. Ikeda and S. Shinkai, *Chem. Rev.*, 1997, **97**, 1713–1734.
16 J. L. Atwood, L. J. Barbour and A. Jerga, *Science*, 2002, **296**, 2367–2369.
17 N. Morohashi and T. Hattori, *J. Inclusion Phenom. Macrocyclic Chem.*, 2018, **90**, 261–277.
18 G. Mislin, E. Graf, M. W. Hosseini and A. De Cian, *J. Chem. Soc., Chem. Commun.*, 1998, 1345–1346.
19 N. Iki, H. Kumagai, N. Morohashi, K. Ejima, M. Hasegawa, S. Miyanari and S. Miyano, *Tetrahedron Lett.*, 1998, **39**, 7559–7562.
20 T. Kajiwara, T. Kobashi, R. Shinagawa, T. Ito, S. Takaishi, M. Yamashita and N. Iki, *Eur. J. Inorg. Chem.*, 2006, 1765–1770.
21 F.-R. Dai, U. Sambasivam, A. J. Hammerstrom and Z. Wang, *J. Am. Chem. Soc.*, 2014, **136**, 7480–7491.
22 N. L. Netzer, F.-R. Dai, Z. Wang and C. Jiang, *Angew. Chem., Int. Ed.*, 2014, **53**, 10965–10969.
23 M. Liu, W. Liao, C. Hu, S. Du and H. Zhang, *Angew. Chem., Int. Ed.*, 2012, **51**, 1585–1588.
24 K. Xiong, F. Jiang, Y. Gai, D. Yuan, L. Chen, M. Wu, K. Su and M. Hong, *Chem. Sci.*, 2012, **1**, 2321–2325.
25 Y. Bi, S. Du and W. Liao, *Coord. Chem. Rev.*, 2014, **276**, 61–72.
26 C.-Z. Sun, L.-J. Cheng, Y. Qiao, L.-Y. Zhang, Z.-N. Chen, F.-R. Dai, W. Lin and Z. Wang, *Dalton Trans.*, 2018, **47**, 10256–10263.
27 F.-R. Dai, D. C. Becht and Z. Wang, *Chem. Commun.*, 2014, **50**, 5385–5387.
28 Y. Jin, H. Jiang, X. Tang, W. Zhang, Y. Liu and Y. Cui, *Dalton Trans.*, 2021, **50**, 8533–8539.
29 S. C. Du, C. H. Hu, J. C. Xiao, H. Q. Tan and W. P. Liao, *Chem. Commun.*, 2012, **48**, 9177–9179.
30 F.-R. Dai and Z. Wang, *J. Am. Chem. Soc.*, 2012, **134**, 8002–8005.
31 F.-R. Dai, U. Sambasivam, A. J. Hammerstrom and Z. Wang, *J. Am. Chem. Soc.*, 2014, **136**, 7480–7491.
32 S. Wang, X. Gao, X. Hang, X. Zhu, H. Han, W. Liao and W. Chen, *J. Am. Chem. Soc.*, 2016, **138**, 16236–16239.
33 Y. Fang, Z. Xiao, J. Li, C. Lollar, L. Liu, X. Lian, S. Yuan, S. Banerjee, P. Zhang and H.-C. Zhou, *Angew. Chem., Int. Ed.*, 2018, **57**, 5283–5287.
34 C. Tan, J. Jiao, Z. Li, Y. Liu, X. Han and Y. Cui, *Angew. Chem., Int. Ed.*, 2018, **57**, 2085–2090.
35 M. R. Dworzak, M. M. Deegan, G. P. A. Yap and E. D. Bloch, *Inorg. Chem.*, 2021, **60**, 5607–5616.
36 M. M. Deegan, T. S. Ahmed, G. P. A. Yap and E. D. Bloch, *Chem. Sci.*, 2020, **11**, 5273–5279.
37 G. R. Lorzing, A. J. Gosselin, B. A. Trump, A. H. P. York, A. Sturluson, C. A. Rowland, G. P. A. Yap, C. M. Brown, C. M. Simon and E. D. Bloch, *J. Am. Chem. Soc.*, 2019, **141**, 12128–12138.
38 X. Hang, B. Liu, X. Zhu, S. Wang, H. Han, W. Liao, Y. Liu and C. Hu, *J. Am. Chem. Soc.*, 2016, **138**, 2969–2972.
39 D. Geng, X. Han, Y. Bi, Y. Qin, Q. Li, L. Huang, K. Zhou, L. Song and Z. Zheng, *Chem. Sci.*, 2018, **9**, 8535–8541.
40 R. Sakamoto, T. Iwashima, M. Tsuchiya, R. Toyoda, R. Matsuoka, J. F. Kögel, S. Kusaka, K. Hoshiko, T. Yagi, T. Nagayama and H. Nishihara, *J. Mater. Chem. A*, 2015, **3**, 15357–15371.
41 R. Matsuoka and T. Nabeshima, *Front. Chem.*, 2018, **6**, 349.
42 S. A. Baudron, *Dalton Trans.*, 2020, **49**, 6161–6175.
43 C. Brückner, Y. Zhang, S. J. Rettigand and D. Dolphin, *Inorg. Chim. Acta*, 1997, **263**, 279–286.
44 S. J. Garibay, J. R. Stork, Z. Wang, S. M. Cohen and S. G. Telfer, *Chem. Commun.*, 2007, 4881–4883.
45 O. V. Dolomanov, L. J. Bourhis, R. J. Gildea, J. A. K. Howard and H. Puschmann, *J. Appl. Crystallogr.*, 2009, **42**, 339–341.
46 A. L. Spek, *Acta Crystallogr., Sect. C: Struct. Chem.*, 2015, **71**, 9–18.
47 A. L. Myers and J. M. Prausnitz, *AIChE J.*, 1965, **11**, 121–127.